A Cu^{I}-Sensing ArsR Family Metal Sensor Protein with a Relaxed Metal Selectivity Profile[†]

Tong Liu,[‡] Xiaohua Chen,[‡] Zhen Ma,[‡,§] Jacob Shokes,[∥] Lars Hemmingsen,[⊥] Robert A. Scott,[∥] and David P. Giedroc*[,‡,§]

Department of Biochemistry and Biophysics, Texas A&M University, College Station, Texas 77843-2128, Department of Chemistry, Indiana University, Bloomington, Indiana 47405-7102, Department of Chemistry, Center for Metalloenzyme Studies, University of Georgia, Athens, Georgia 30602-2556, and Department of Natural Science, The Royal Veterinary and Agricultural University, Thovaldsensvej 40, DK-1871 Fredericksberg C, Denmark

Received July 11, 2008; Revised Manuscript Received August 8, 2008

ABSTRACT: ArsR (or ArsR/SmtB) family metalloregulatory homodimeric repressors collectively respond to a wide range of metal ion inducers in regulating homeostasis and resistance of essential and nonessential metal ions in bacteria. BxmR from the cyanobacterium *Osciliatoria brevis* is the first characterized ArsR protein that senses both Cu^{I}/Ag^{I} and divalent metals Zn^{II}/Cd^{II} in cells by regulating the expression of a P-type ATPase efflux pump (Bxa1) and an intracellular metallothionein (BmtA). We show here that both pairs of predicted α3N and α5 sites bind metal ions, but with distinct physicochemical and functional metal specificities. Inactivation of the thiophilic α3N site via mutation (C77S) abolishes regulation by both Cd^{II} and Cu^{I}, while Zn^{II} remains a potent allosteric negative effector of operator/promoter binding ($\Delta G_c \geq +3.2$ kcal mol^{-1}). In contrast, α5 site mutant retains regulation by all four metal ions, albeit with a smaller coupling free energy ($\Delta G_c \approx +1.7$ (± 0.1) kcal mol^{-1}). Unlike the other metals ions, the BxmR dimer binds 4 mol equiv of Cu^{I} to form an α3N binuclear $Cu^{I}_2S_4$ cluster by X-ray absorption spectroscopy. BxmR is thus distinguishable from other closely related ArsR family sensors, in having evolved a metalloregulatory α3N site that can adopt an expanded range of coordination chemistries while maintaining redundancy in the response to Zn^{II}. The evolutionary implications of these findings for the ArsR metal sensor family are discussed.

All cells must obtain their quota of biologically required transition metal ions for use as cofactors in metalloenzymes or for structural or regulatory roles through specific membrane-associated transporters or uptake systems (*9*). However, all metal ions are toxic in excess, and the intracellular availability of each is tightly controlled in such a way that metal homeostasis allows organisms to rapidly respond to changes in their microenvironments (*10, 11*). Likewise, metal ions that play no biological role, e.g., heavy metal pollutants and other environmental contaminants, must be detoxified via biotransformation or efflux from the cytosol (*12, 13*).

This adaptive response is mediated by gene regulatory proteins, coined metalloregulatory proteins (*10*), or metal sensor (*14*) proteins. These specialized proteins have evolved metal coordination sites that "sense" specific metal ion(s) in the cytosol by forming specific coordination complexes. This, in turn, functions to activate or inhibit DNA binding to operator sites(s) in the promoter, thereby regulating the expression of genes. These genes include transporters, intracellular chelators, and detoxification enzymes that mediate metal homeostasis or resistance in what is thought to be a selective adaptive response.

There are currently seven major families of metal-sensing transcriptional regulators that have thus far been structurally characterized in prokaryotes (see ref *14* for a review). These seven families span the detection of the six primary biologically essential first row transition elements Mn^{II}, Fe^{II}, Co^{II}, Ni^{II}, Cu^{I}, and Zn^{II}, as well as nonbiological heavy metals Ag^{I}/Au^{I} and Cd^{II}/Hg^{II}, respectively, found in the environment. In addition, ArsR[1] or ArsR/SmtB (*6*) and MerR (*15*) family sensors have been identified that detect Pb^{II}, as well as As^{III}/Sb^{III} and Bi^{III}. Sensor families are typically named for the founding member(s) that gave rise to the family (*14*). Of interest here is the ArsR/SmtB family, named for *E. coli* R774 ArsR, which regulates expression of the *ars* operon in response to trivalent As^{III} and Sb^{III} and their oxyanions and organoarsenicals (*16*) and the Zn^{II} sensor *Synechococcus* SmtB (*17*), which regulates expression of the *smt* (*Synechococcus m*etallo*t*hionein) operon largely as a result of Zn^{II} toxicity.

[†] This work was supported by grants from the National Institutes of Health (GM042569) and the Robert A. Welch Foundation (A-1295) to D.P.G.

* To whom correspondence should be addressed. E-mail: giedroc@indiana.edu. Tel: 812-856-5449. Fax: 812-856-5710.

[‡] Texas A&M University.

[§] Indiana University.

[∥] University of Georgia.

[⊥] The Royal Veterinary and Agricultural University.

[1] Abbreviations: BxmR, *Oscillatoria brevis* CPx-ATPase metal-regulated repressor; Bxa1, *O. brevis* CPx-ATPase-1; BmtA, *O. brevis* metallothionein-A; ArsR, arsenic repressor; mag-fura-2, 2-[6-[bis(carboxymethyl)amino]-5-(carboxymethoxy)-2-benzofuranyl]-5-oxazolecarboxylic acid; quin-2, *N*-(2-((8-(bis(carboxymethyl)amino)-6-methoxy-2-quinolinyl)methoxy)-4-methylphenyl)-*N*-(carboxymethyl)glycine; NQI, nuclear quadrupole interaction.

10.1021/bi801313y CCC: $40.75
Published on Web 09/17/2008

ArsR family sensors (COG0640) constitute a very large class of bacterial transcriptional regulators. A recent report identifies over 500 unique sequences that could be divided into eight major groups on the basis of global sequence similarity (*7*). A least four structurally distinct, subunit-bridging metal sensing sites have now been identified and characterized in ArsR family sensors, a remarkable collective feature that appears to distinguish the ArsR family from all other metalloregulatory protein classes (*4, 14*). In other metal sensor families, a single regulatory metal site often acquires distinct metal specificities by more subtle structural alterations in the first coordination shell (*14, 18, 19*), a feature that also characterizes ArsR sensors that harbor a single subtype of metal site, e.g., α5/α5C (see below) (*20*).

In ArsR family proteins, metal sites are named for the secondary structural elements that are known or predicted to provide ligand donor atoms to the individual metal ions (*20, 21*). These sites have been designated α3N/α3 (*21*) (or metal site 1 in *S. aureus* pI258 CadC (*1*)), α4C (*22*), α5/α5C (*3, 21, 23*) (site 2 in *S. aureus* pI258 CadC), and most recently α5-3 (*7*).[2] Further evidence for an even greater structural diversity of sensing sites in ArsR family proteins comes from the recent characterization of two As^{III}-sensing ArsRs shown to harbor *tris*-thiolato As^{III} binding sites distinct from the S_3 α3 site originally characterized in *E. coli* R773 ArsR (*4, 5*). Similarly, our physical characterization of a predicted Cd^{II}/Pb^{II}-sensing CmtR from *Streptomyces coelicoler* (SCO0875) reveals a second S_3 Cd^{II}/Pb^{II} binding site involving a pair of adjacent Cys residues at the extreme C-terminus (Y. Wang and D. Giedroc, unpublished observations) in addition to the canonical α4C Cd^{II}/Pb^{II} site structurally characterized (*24, 25*).

While the metal selectivity of individual metal site subtypes is rather well understood and sometimes predictable on the basis of the amino acid sequence (*20, 26*), approximately half of the projected ArsR family members do not conform to any of these four metal binding motifs. For example, one poorly characterized subgroup contains a conserved Met and two conserved Cys, the latter derived from the projected α2 and α5 helices that are predicted to be quite close in the structure but may not bind metal ions directly (*7, 27*). These include *Paracoccus pantotrophus* SoxR, the thiosulfate-induced sulfur-oxidizing (*sox*) operon regulator (*28*), *V. cholerae* HyU (*7*), and *Xylella fastidiosa* BigR, a regulator implicated biofilm formation (*29*). Thus, it remains a considerable challenge to unambiguously identify the mode of induction of ArsR sensors that do not precisely conform to one of the four known structural classes on the basis of amino acid sequence alone. In addition, since some ArsR family sensors contain two metal sites, e.g., α3N and α5 (*6, 30*), a further complication is that one site might be metalloregulatory while the other site may bind metal ions but in a way that does not mediate allosteric regulation of DNA binding and is thus nonfunctional (*30, 31*).

Initial biological studies established that an ArsR family repressor, termed BxmR,[1] regulated the expression of genes encoding both a heavy metal transporting ATPase, Bxa1,[1] and an intracellular metallothionein, BmtA,[1] in the freshwater cyanobacterium *Oscillatoria brevis* (*32, 33*). *Oscillatoria* spp. produce geosmin and 2-methylisoborneaol which give drinking water a musty or earthy odor and have a major negative economic impact on the catfish aquaculture industry due to absorption in the flesh of the fish (*34*). Copper sulfate has been extensively used in water purification systems as a copper algaecide (*34*), and it was subsequently demonstrated that *bxa1* expression was inducible by both monovalent (Cu^I/Ag^I) and divalent (Zn^{II}/Cd^{II}) ions in *O. brevis*, a novel property (*33*). The thiol oxidant diamide is also an inducer of *bmtA* expression (*35*). *In vitro* DNA binding and coupled transcription-translation experiments suggested that metal and diamide stress-induced disassembly of BxmR-operator/promoter complexes was directly responsible for regulation (*35, 36*).

In this report, we present a comprehensive characterization of the metal binding properties and metalloregulation of *bxa1* operator/promoter binding by BxmR (*33*). We show that both pairs of predicted α3N and α5 sites bind metal ions, but with distinct physicochemical and functional metal specificities. BxmR is thus distinguished from other closely related ArsR family sensors, in having evolved a metalloregulatory α3N site that can adopt an expanded range of coordination chemistries to include Cu^I/Ag^I, while maintaining redundancy in the response to Zn^{II}. These studies provide a glimpse as to how an ArsR family metal sensor with a relaxed metal specificity profile could have evolved to effect resistance against an expanded range of heavy metal ions.

EXPERIMENTAL PROCEDURES

Construction of E. coli Overexpression Plasmids for BxmRs and Protein Purification. The wild-type *bxmR*-coding region was amplified by PCR from *O. brevis* genomic DNA and cloned into pET3a (Novagen) between the *Nde*I and *Eco*RI restriction sites to construct pET3a-BxmR. In order to obtain overexpression clones for α3NΔ and α5Δ BxmRs, a PCR-based quick-change mutagenesis method was employed to replace Cys77 to Ser in the α3N site, or ^{132}HLDEE^{136} to ^{132}NLTYA^{136} (H132N/D134T/E135Y/E136A) in the α5 site, using pET3a-BxmR as a template to create pET3a-α3NΔ BxmR and pET3a-α5Δ BxmR, respectively. C31S BxmR was prepared in exactly the same way. The integrity of all plasmid constructions was confirmed by complete DNA sequencing.

The resultant constructs were transformed into *E. coli* BL21(DE3) and grown in LB to midlog phase, after which time 0.4 mM IPTG was added and cells were allowed to grow for an additional 2.5 h. Freshly harvested cells were pelleted by low-speed centrifugations and suspended in 100 mL of buffer A (25 mM MES, 5 mM DTT, 1 mM EDTA, pH 6.0) and lysed by sonication. The cellular lysate was centrifuged and the supernatant pooled and subjected to precipitation by addition of polyethylenimine (PEI) to 0.15% (v/v) at pH 6.0. The PEI supernatant and precipitated fractions were collected separately. The PEI pellet was resuspended in buffer A containing 0.50 M NaCl to extract bound proteins. Protein fractions derived from the NaCl-washed PEI pellet were precipitated by the addition of solid $(NH_4)_2SO_4$ to 50% saturation. Each ammonium sulfate pellet

[2] *S. aureus* pI258 CadC (*1*) contains an additional N-terminal α-helix relative to zinc sensors *Synechococcus* SmtB and *S. aureus* CzrA (*2, 3*). Thus the helical designations α1−α5 in SmtB correspond to helices α2−α6 in CadC and ArsRs recently characterized (*4, 5*). The designation of metal sites used here, e.g., α3N, conforms to the SmtB/CzrA secondary structure convention used in nearly all of the previous work (*6, 7*).

was gently resuspended in 100 mL of buffer A with 0.05 M NaCl and separately subjected to SP Fast Flow chromatography (20 mL bed volume) on an Äkta-10 purifier, with elution achieved with a linear NaCl gradient (0.05−0.75 M) in buffer A. BxmR-containing fractions eluted at approximately 0.15 M NaCl and 0.35 M NaCl and were pooled separately. The resultant protein fractions were further purified by Superdex 75 size-exclusion chromatography and anion-exchange HPLC using a procedure similar to that described previously (*8*). Individual fractions containing highly purified BxmR were pooled, concentrated, and dialyzed against 3 L of buffer B (10 mM HEPES, 0.40 M NaCl, pH 7.0) in an anaerobic Vacuum Atmospheres glovebox. The purity of the final products was estimated by visualization of Coomassie-stained 18% Tris−glycine SDS−PAGE gels to be ≥95%. The concentrations of all BxmR stock solutions were determined by quantitative amino acid analysis carried out by the Texas A&M University Protein Chemistry Laboratory. The number of reduced thiols in wild-type BxmR was determined by anaerobic DTNB colorimetric assay to be 4.1 (4.0 expected) and 2.8 (3 expected) in the WT and C31S BxmRs (*8*). The possible presence of copper in apo-BxmR was determined using a Perkin-Elmer AAnalyst 700 atomic absorption spectrophotometer operating in the flame mode using hollow cathode lamps specific for each metal (*37*). The purification of α3NΔ (C77S) and α5Δ BxmRs was performed in essentially the same fashion and characterized as indicated.

Copper Binding Experiments. All metal binding experiments were carried out anaerobically at ambient temperature (≈22 °C) using either a Hewlett-Packard Model 8452A spectrophotometer (for UV−vis electronic absorption spectra) or at 25 (±0.1) °C with an ISS PC1 photon counting spectrofluorometer (for fluorescence and luminescence titrations, respectively) essentially as described previously (*37, 38*). Solution conditions were 10 mM MES and 0.1 M NaCl, pH 6.3, unless otherwise indicated. 10.5 and 11.2 μM wild-type and C31S BxmR monomer, respectively, were used for the UV−vis absorption experiments, while 10.0 μM BxmR monomer was used for the luminescence experiments (λ_{ex} = 300 nm with the emission spectrum scanned from 500 to 750 nm). For tyrosine fluorescence measurements, 5.0 μM BxmR monomer in buffer B (10 mM HEPES, 0.40 M NaCl, pH 7.0) either was titrated with 2−5 μL aliquots of a 400 μM Cu^{I} stock in buffer B or mock-titrated with buffer B (λ_{ex} = 280 nm; λ_{em} = 305 nm). At each *i*th addition, the emission intensity was recorded and corrected for dilution, photobleaching (from the mock-titrated sample), and the inner filter effect exactly as described previously (*21*).

Other Metal Binding Experiments. Zn^{II} binding stoichiometries and affinities of wild-type, α3NΔ, and α5Δ BxmRs were determined using chelator competition assays with either mag-fura-2[1] (K_{Zn} = 5.0 × 10^7 M^{-1} at pH 7.0) (*39*) or quin-2[1] (K_{Zn} = 2.7 × 10^{11} M^{-1} at pH 7.0, 25 °C) (*40*) using absorption spectroscopy essentially as described (*23, 41*). These data were fit using a competitive binding model with DynaFit (*42*) to determine stepwise zinc binding affinities, K_{Zni}. For mag-fura-2 experiments, 25 μM BxmR dimer (12.5 μM monomer) was mixed with 16.0 μM mag-fura-2 and titrated with a known stock solution of Zn^{II}; for quin-2 experiments, 20 μM BxmR dimer was mixed with 15 μM quin-2 and titrated with Zn^{II} (see Table 1). Co^{II} and Cd^{II} binding experiments were carried out essentially as described previously (*30, 43*) with the solution conditions given in the figure legends. The metal concentration of all metal titrants used in individual experiments was quantified by atomic absorption spectroscopy as described (*8*).

Table 1: Stepwise Zinc Binding Affinities, K_{Zni}, Derived from mag-fura-2 and quin-2 Chelator Competition Experiments[a]

BxmR protein	chelator	K_{Zn1} (M^{-1})	K_{Zn2} (M^{-1})	K_{Zn3} (M^{-1})	K_{Zn4} (M^{-1})
wild type	mag-fura-2	≥10^9 [a]	≥10^9	2.2 × 10^7	nd[b]
	quin-2	9.4 × 10^{12}	1.1 × 10^{12}	nd[c]	nd[c]
α3NΔ	mag-fura-2	≥10^9 [a]	6.0 × 10^7		
	quin-2	6.4 × 10^{12}	nd[c]		
α5Δ	mag-fura-2	≥10^9 [a]	3.0 × 10^6		
	quin-2	4.6 × 10^{10}	nd[c]		

[a] From nonlinear least-squares fits to data like those shown in Figure 2 to a model assuming four (wild type) or two (α3NΔ and α5Δ) stepwise binding events to a nondissociable dimer, each characterized by an affinity of K_{Zni}. [b] nd, binding not detected, or $K_{Zni} \leq 10^5$ M^{-1} (a lower limit for mag-fura-2). [c] nd, binding not detected, or $K_{Zni} \leq 10^9$ M^{-1} (a lower limit for quin-2).

Fluorescence Anisotropy-Based DNA Binding Experiments. These experiments were carried out essentially as described previously (*23, 41*) using an ISS PC1 spectrofluorometer fitted with polarizers in the L format. 52 base pair oligonucleotide duplexes were prepared by mixing one unlabeled "bottom" strand at a slight excess relative to a 5′-fluorescein labeled "top" strand, annealed by heating to 95 °C and slow-cooling at room temperature. Duplexes corresponding to the *bxa1* and *bxmR* operator-promoter (O/P) regions contained a 26 base pair TGAA-containing inverted repeat (see ref *36* for sequences) centered in the 52 base pair duplex. Titrations were carried out with 10 nM duplex in buffer B (10 mM Hepes, 0.4 M NaCl, pH 7.0, 1.0 mM dithiothreitol) at 25 (±0.1) °C with either apo-BxmRs or BxmRs preincubated with the indicated amount of a metal ion, e.g., Cu^{I}, Ag^{I}, Zn^{II}, or Cd^{II}. Experimental binding curves were fit using DynaFit (*42*) to a binding model that assumes that two dimers bind to the DNA with identical binding affinities ($K_1 = K_2$) (*36*), linked to a monomer−dimer equilibrium constant, K_{dim}, of 5.0 × 10^6 M^{-1} (*44*). The characteristic anisotropy of the 2:1 dimer:DNA species, $r_{(P2)2D}$, was optimized during the fit, with the $r_{(P2)\ D}$ value fixed to exactly halfway between $r_{(P2)2D}$ and r_D. In this work, the allosteric coupling free energy, ΔG_c, was operationally defined as the logarithmic ratio K_1^{metal}/K_1^{apo} according to $\Delta G_c = -RT \ln(K_1^{metal}/K_1^{apo})$ with T = 298 K.

RESULTS

Sequence Alignment of Selected ArsR Regulators. O. brevis BxmR contains complete predicted ligand donor sets for both the interprotomer α3N and α5 metal sites previously characterized in other ArsR family sensors (*6, 21*). The α3N site is thiophilic site with a diagnostic ^{75}CVC^{77} metal binding sequence (*30*) and a number of potential donor residues in the N-terminal region, including by Cys23, His27, and Cys31 (*36*); the multiple sequence alignment of α3N sensors reveals that Cys31 in BxmR is unique (Figure 1). Cys23, Cys31, Cys75, and Cys77 are the only Cys in BxmR. The α5 site is a well-characterized tetrahedral Zn^{II}-sensing site composed of carboxylate and imidazole ligands (*3, 23*); in BxmR, these are Asp119, His121, His132′, and Glu135′ with the His

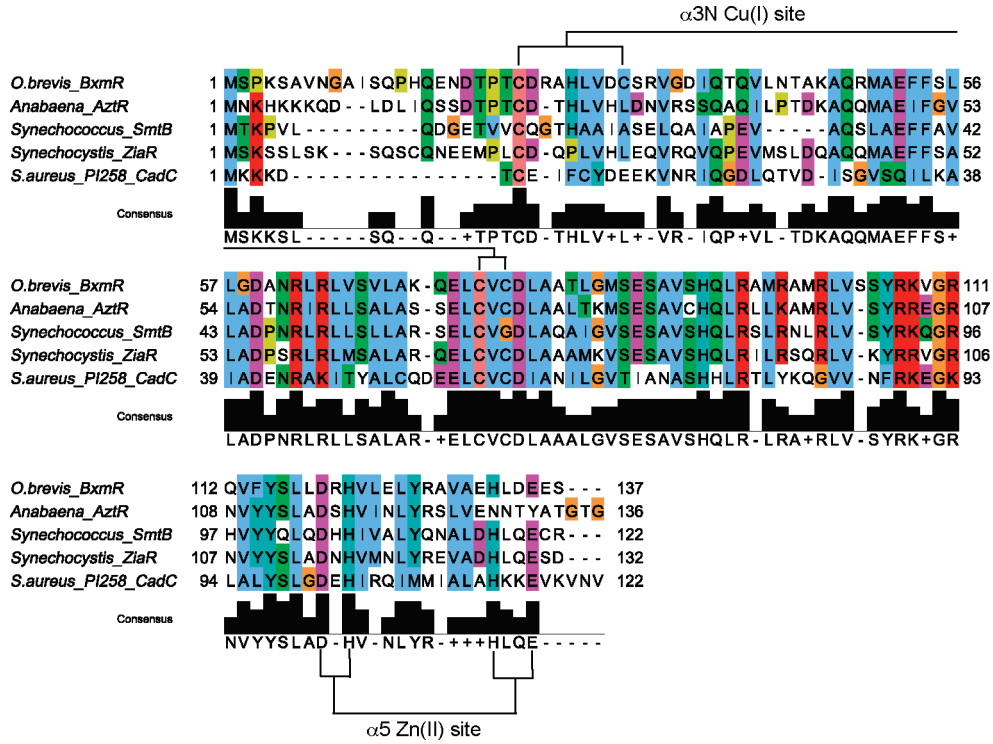

FIGURE 1: Multiple sequence alignment of BxmR with other ArsR/SmtB family divalent metal ion-sensing regulatory transcriptional repressors (*6, 8, 21, 30, 52*). The proposed primary Cu^{I} binding ligands in the α3N site and α5 site for Zn^{II} are indicated for BxmR (this work).

corresponding to His132 the key allosteric residue in other Zn^{II} sensors CzrA and SmtB (*23*). α3NΔ BxmR corresponds to C77S BxmR; an analogous nonmetal liganding substitution abolishes Cd^{II} binding and sensing by *S. aureus* CadC (*30, 45*) and Cd^{II}/Zn^{II} sensing by *Anabaena* AztR (*8*). α5Δ BxmR is a quadruple mutant (H132N/D134T/E135Y/E136A) that changes two of the four α5 site ligands, His132 and Glu135, to nonmetal liganding residues found in *Anabaena* AztR (*8*); these substitutions abolish Zn^{II}/Co^{II} binding to this site in AztR.

Zn^{II} Binding by Wild-Type, α3NΔ, and α5Δ BxmRs. Like other previously characterized ArsR sensors (*20, 44*), BxmR is a stable dimer in solution as revealed by dynamic light scattering and gel filtration chromatography (data not shown). As a result, wild-type BxmR is predicted to contain four subunit-bridging metal binding sites per dimer (or two per protomer), two α3N and two α5 sites. We used standard dye competition experiments with two different chelators of widely different affinities, mag-fura-2 ($K_{Zn} = 5.0 \times 10^7\ M^{-1}$) and quin-2 ($K_{Zn} = 2.7 \times 10^{11}\ M^{-1}$), in order to quantify the stoiochiometry and affinity of the Zn^{II} binding sites in wild-type, α3NΔ, and α5Δ BxmRs (*3, 21*). Representative mag-fura-2 and quin-2 competition titrations carried out with wild-type BxmR are shown in Figure 2, with parameter values obtained from a simple stepwise binding model shown in Table 1 for all BxmR species investigated here. Wild-type BxmR binds three Zn^{II} ions with an affinity that is either comparable to, or far greater than, that of mag-fura-2, with the fourth site transparent in this assay ($K_{Zn} \leq 10^5\ M^{-1}$) (Table 1). Using the higher affinity competitor dye, quin-2, reveals just two high affinity sites, with K_{Zn} values of $\approx 10^{13}$ and $10^{12}\ M^{-1}$; this result is consistent with the mag-fura-2 titrations. Carrying out the same experiments with α3NΔ and α5Δ BxmRs, where one pair of symmetry-related metal

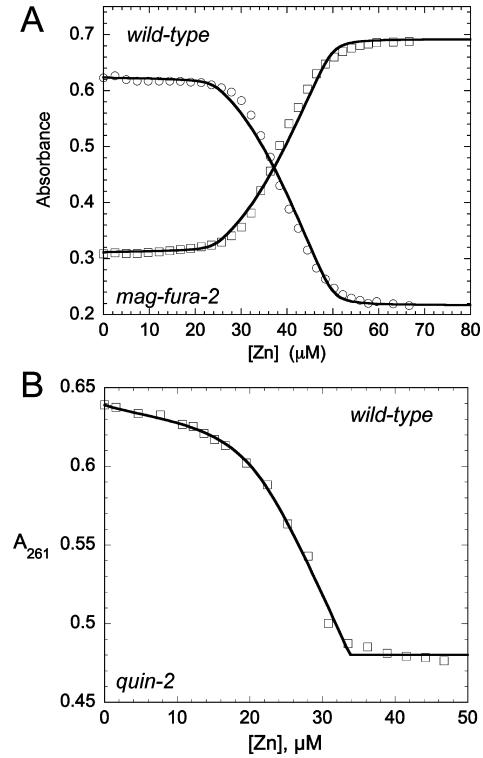

FIGURE 2: Zn^{II} binding by wild-type BxmR homodimer. (A) Titration of a mixture of 25 μM (monomer) BxmR and 16 μM mag-fura-2 with Zn^{II} with the absorption monitored simultaneously at 366 nm (open circles) and 325 nm (open squares). (B) Titration of a mixture of 20 μM (monomer) BxmR and 15 μM quin-2 with Zn^{II}, with the absorption monitored at 261 nm. In both cases, the solid lines represent a fit to a multiple site binding model, with the parameters compiled in Table 1. Analogous titrations were carried out with α3NΔ and α5Δ BxmRs under the same conditions (see Supporting Information Figure S1) with these parameters compiled in Table 1.

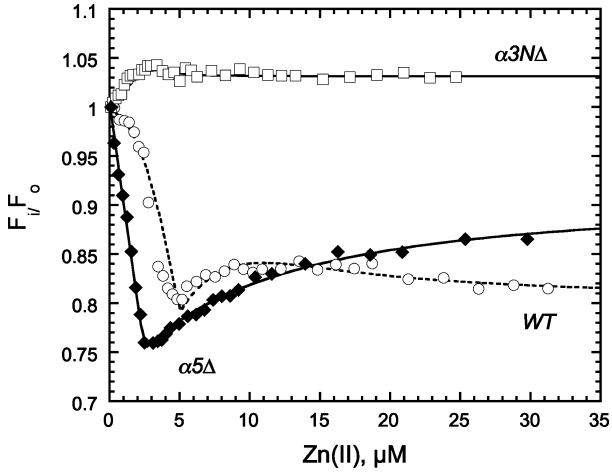

FIGURE 3: Anaerobic titration of 5.0 μM wild-type BxmR monomer (2.5 μM dimer) (○), α3NΔ (□), and α5Δ (◆) BxmRs with Zn^{II} as monitored by change in the Tyr fluorescence intensity, F_i/F_o. The solid lines through the data correspond to a nonlinear least-squares fit to the model that invokes sequential binding of Zn^{II} to a single high-affinity site (for α3NΔ and α5Δ BxmRs) or two high-affinity sites (for wild-type BxmR) each with a characteristic F_i/F_o signature. After filling these high-affinity zinc binding sites (one α5 site with an $F_i/F_o > 1$; one α3N site with an $F_i/F_o < 1$), Zn(II) binds to each of the remaining low-affinity α5′ and α3N′ sites on the dimer. Fitted parameters are as follows, with $K_{Zn1} > 10^{10}$ M^{-1} (see Figure 2A and Table 1): α3NΔ BxmR, F_i/F_o values 1.045 (±0.001) and 1.03 (fixed) for the high-affinity and low-affinity α5 Zn(II) sites, respectively; α5Δ BxmR, F_i/F_o values 0.753 (±0.002) and 0.915 (±0.011) for the high-affinity and low-affinity α3N Zn(II) sites, respectively; wild-type BxmR, F_i/F_o constrained to the above values for first three binding steps, with F_i/F_o for filling the final binding site 0.80 (±0.03).

sites is inactivated in each case, clearly shows that each mutant binds two metal ions, one with very high affinity ($K_{Zn} > 10^9$ M^{-1}), measurable with quin-2 (Table 1), and one with an affinity comparable to or less than that of mag-fura-2 ($K_{Zn} \leq 10^7$ M^{-1}) (see Supporting Information Figure S1 and Table 1). These binding parameters are diagnostic for strong negative homotropic cooperativity of Zn^{II} binding to each pair of metal sites, previously documented in the α3N sensor CadC (*44*) and structurally validated in the α5 sensors CzrA (*3, 41*) and SmtB (*21*).

Taking all of the data together, the simplest interpretation is that Zn^{II} fills the metal binding sites on the wild-type BxmR homodimer in the following order: α5 ∼ α3N ⟹ α5′ ∼ α3N′. Thus, one of the α5 sites and one of the α3N sites possess very high intrinsic zinc affinities $K_{Zn} \geq 10^{12}$ M^{-1} or nearly equivalent to that found previously in the Zn^{II} sensor CzrA (*3, 41*); as a result, the dominant Zn^{II} complex that would persist over a wide range of $[Zn^{II}]_{free}$ is the BxmR $\alpha5_1/\alpha3N_1$ homodimer. Further evidence for this formation of an $\alpha5_1/\alpha3N_1$ metalated homodimer comes from Zn^{II} binding isotherms monitored by a change in the steady-state Tyr fluorescence of 5.0 μM BxmRs (Figure 3). BxmR contains the same three Tyr residues found in the known structure of SmtB (*2, 3*), two in each strand of the β-wing and one in the α5 helix (Figure 1). As previously found for SmtB, Zn^{II} binding to the α5 site in α3NΔ BxmR gives rise to small but measurable enhancement or increase in the Tyr fluorescence intensity (*21*). In contrast, binding to the α3N site in α5Δ BxmR gives rise to the large quenching of the Tyr fluorescence not observed in SmtB; this spectral change is likely reporting on changes in the β-wing conformation due to α3N site binding. Both α3NΔ and α5Δ BxmR Zn^{II} binding isotherms reach maximum (or minimum) F/F_o values at ≈0.5:1 Zn^{II} to monomer consistent with the idea that half the sites drive the conformational change in the dimer as found previously for the α5 site in CzrA (*41*). Further, the conformational changes may well be distinct since the fluorescence yields of Tyr are different in each case. Strikingly, the addition of Zn^{II} to wild-type BxmR gives rise to a binding curve that is best described as a linear combination of Zn^{II} bound to either the α5 or α3N site, i.e., added Zn^{II} partitions between the two sites, which then reaches a minimum F/F_o value at ≈1:1 Zn^{II} to monomer (2 per dimer); residual binding of the third Zn^{II} to the second α3N site results in a small upward curvature of the F/F_o values (Figure 3).

Co^{II} Binding by Wild-Type BxmR. While Co^{II} is not an inducer of the *bxa1* or *bmtA* genes (*36*), Co^{II} is often used as a structural surrogate for Zn^{II} to obtain insight into coordination geometry and nature of the ligand donor atoms. Interestingly, the sequence of metal binding steps for Zn^{II} is in contrast to that observed for Co^{II}, which largely fills both α5 sites, followed by both α3N sites in wild-type BxmR, an interpretation facilitated by the distinct spectral features of the Co^{II} complexes of the α5 and α3N sites (*8, 21, 30*) (Supporting Information Figure S2). Both sites adopt tetrahedral or distorted tetrahedral coordination geometries consistent with S_3(N/O) α3N and N_2O_2 α5 ligand donor sets (*8, 21*). As expected, addition of stoichiometric Zn^{II} effectively bleaches the Co^{II}-α5 visible absorption spectrum in α3NΔ BxmR, consistent with $K_{Zn}^{\alpha5} \gg K_{Co}^{\alpha5}$ as expected for tetrahedral symmetry (*43*).

Cd^{II} Binding by Wild-Type, C31S, α3NΔ, and α5Δ BxmRs. Representative Cd^{II} binding curves are shown for wild-type and C31S BxmRs as monitored by Cys $S^- \Longrightarrow Cd^{II}$ ligand-to-metal (or metal-to-ligand) charge transfer absorption at 235 nm (Supporting Information Figure S3). The binding curves in both cases are essentially stoichiometric and reveal a single Cd^{II} binding site per monomer (2 per dimer) characterized by a molar absorptivity at 235 nm of ≈20000 M^{-1} cm^{-1} for wild-type BxmR, most consistent with a tetrahedral S_4 complex (*30*). This binding curve is reporting on filling of the α3N sites with Cd^{II}, with any binding to the carboxy-terminal α5 sites not detected in this assay since this site contains no thiolate ligands. Cd^{II} does bind here, but with a lower affinity than Co^{II} since a 4-fold molar excess of Cd^{II} retains significant Co^{II} absorption deriving from the α5 site in α3NΔ BxmR (data not shown). Since we observe a lower molar absorptivity with the C31S BxmR (ϵ_{235} = 16000 M_{Cd}^{-1} cm^{-1}), the simplest interpretation is that Cd^{II} coordinates to all four Cys in BxmR (Cys23, Cys31, Cys75, Cys77) to create a distorted tetrahedral S_4 site. As expected from prior studies of CadC (*30, 46*), Cd^{II} binds to the mutant α3N sites in α3NΔ BxmR, but with a lower affinity and lower molar absorptivity (ϵ_{235} = 7000 M^{-1} cm^{-1}); this is indicative of a significantly perturbed first coordination shell (data not shown).

Cu^{I} Binding by Wild-Type, C31S, and α5ΔBxmRs. Previous studies have established expression of both the *bxa1* and *bmtA* genes is responsive to Cu/Ag and that the addition of reduced Cu^{I} or Ag^{I} to preformed BxmR-*bxa1* and BxmR-*bxmR/bmtA* operator-promoter fragments *in vitro* resulted in dissociation of these complexes (*36*). Although these results

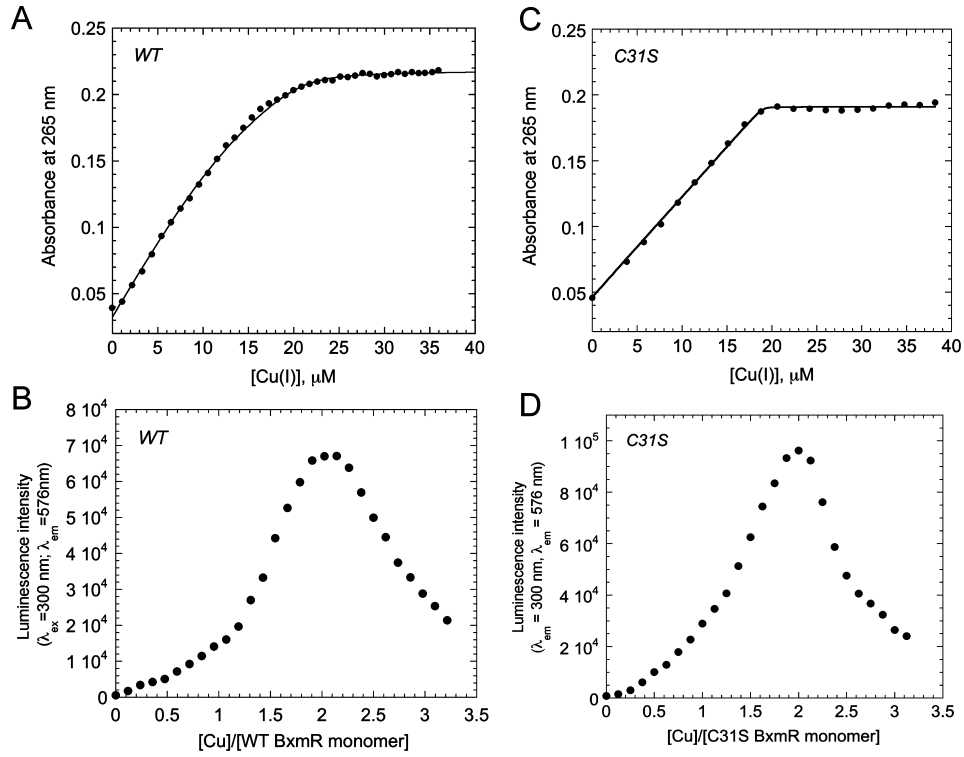

FIGURE 4: Anaerobic Cu^I binding properties of 10.5 μM (monomer) WT BxmR (panels A and B) and 11.2 μM (monomer) (panel C) or 10.0 μM C31S BxmR (monomer) (panel D) as monitored by UV absorption at 265 nm (panels A and C) or Cu^I luminescence (panels B and D) (*38*). Conditions: 10 mM Mes, 0.1 M NaCl, pH 6.3.

are consistent with a functionally important and direct interaction of the Cu^I/Ag^I with BxmR, they provided no insight into the nature of the coordination complexes formed by Cu^I/Ag^I.

We measured Cu^I binding to apo forms of wild-type and C31S BxmR anerobically using two different spectroscopic techniques. These include UV−visible absorption which reports on Cys $S^- \Longrightarrow Cu^I$ ligand-to-metal charge transfer absorption (LMCTs), i.e., formation of cysteine−copper coordination bonds, and luminescence in the visible region (λ_{ex} = 300 nm, λ_{em} = 580 nm). The results of these experiments are shown for wild-type and C31S BxmRs in Figure 4A,B and Figure 4C,D, respectively. Cu^I binding isotherms monitored in the UV region are consistent with a limiting stoichiometry of two Cu^I/monomer or four per dimer in both cases (Figure 4A,C). While the C31S Cu^I binding curve is essentially stoichiometric under these conditions (pH 6.3, 25 °C), the binding curve for wild-type BxmR can be fit to two stepwise equilibrium binding affinities, K_{Cu1} and K_{Cu2} of 3.6×10^7 M^{-1} and 2.7×10^6 M^{-1}. The luminescence spectra are also consistent with a limiting stoichiometry of 2.0 Cu^I/monomer (4 per dimer) as judged by the point at which the maximum luminescence is obtained. At excess Cu^I, the luminescence intensity decreases significantly which is likely reporting on rearrangement of the chelate to a less solvent shielded environment concomitant with the formation of nonnative multinuclear copper clusters (*38*). This feature also characterizes Cu^I binding to some but not all unrelated copper regulatory proteins known to form multinuclear copper clusters (*38, 47*), but not in a mononuclear site of relatively low luminescence intensity (*37*). We see virtually the same luminescence titration curve with α5Δ BxmR (data not shown), revealing that, not surprisingly, the carboxylate/imidazole-containing α5 site does not bind Cu^I, at least in a way that contributes to the luminescence intensity. Thus, unlike the case for the Zn^{II}/Cd^{II}, these studies reveal that the α3N site of wild-type and C31S BxmRs binds Cu^I with a maximal stoichiometry of 2:1 (4 per dimer). We also note the Cu^I-saturated forms of wild-type and C31S BxmR contain a fully accessible α5 site since each is capable of binding Co^{II} to this site (Supporting Information Figure S4); this result suggests that these two classes of metal sites are structurally independent.

BxmR Forms a Binuclear Cu^I_2−S_4 Complex. Copper K-edge X-ray absorption spectroscopy (XAS) was used to investigate the structure of the wild-type Cu^I complex formed at a 2:1 Cu^I:BxmR monomer molar ratio, and compared with that formed by C31S and α5Δ BxmRs, both at 1:1 metal:monomer ratios. The near-edge spectra of all three samples are essentially superimposable, and each is fully compatible with an average trigonally coordinated cuprous (Cu^I) ion (Figure 5A) (*37*). Experimental copper K-edge extended X-ray absorption fine structure (EXAFS) spectra are shown in the inset to Figure 5B with Fourier transforms of these data shown in the main body of the figure; structural parameters derived from the EXAFS curve fitting are compiled in Supporting Information Table S1. Virtually identical coordination environments are obtained for all three samples, and each is well described by three Cu−S interactions at 2.25−2.26 Å and an intense Cu−Cu scattering peak at ≈2.70 Å. These spectra are therefore consistent with a limiting Cu^I_2−S_4 complex, involving all four Cys of BxmR (Cys23, Cys31, Cys75, and Cys77) in wild-type and α5Δ BxmRs. Since the XAS near-edge and EXAFS spectra are virtually identical at saturating Cu^I for C31S BxmR, this suggests that if Cys31 does indeed donate a thiolate ligand, it can be readily replaced with a molecule from solvent (H_2O or Cl^-; note that Cl^- cannot be distinguished from S^-) (*30*),

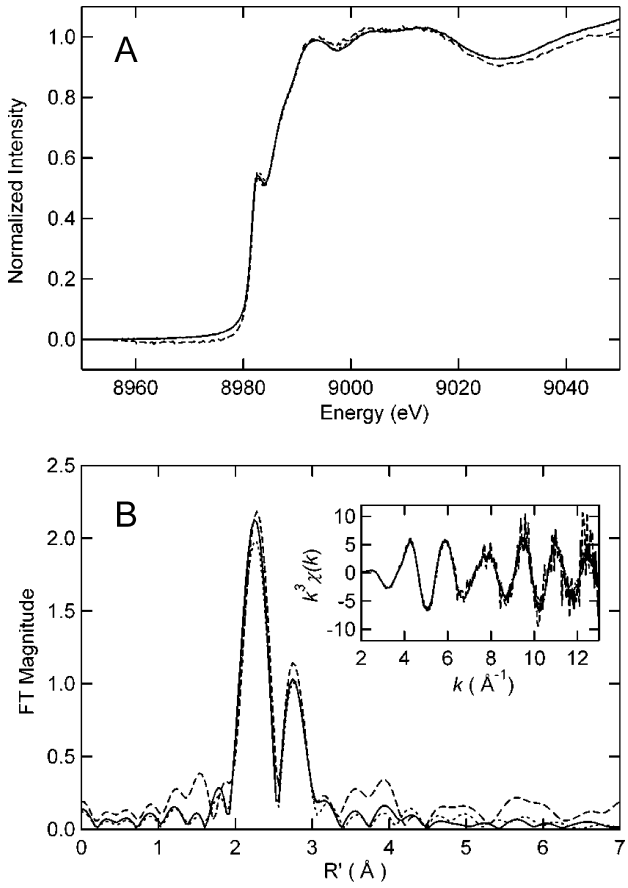

FIGURE 5: X-ray absorption spectroscopy of Cu-BxmRs. (A) Cu K-edge X-ray absorption near-edge spectra of WT BxmR (solid line), α5Δ BxmR (dashed line), and C31S BxmR (dotted line). (B) Cu-S phase-corrected EXAFS Fourier transforms of WT BxmR (solid line), α5Δ BxmR (dashed line), and C31S BxmR (dotted line). Inset: k^3-weighted EXAFS spectra for each Cu^I complex. Parameters that derive fitting these data to various coordination models are compiled in Supporting Information Table S1.

the Ser side chain itself, or another side chain, e.g., His27 (see Figure 1). It is important to note that XAS near-edge and EXAFS spectra derived from coordination by a single His within a tetracopper $Cu^I_4-S_5N$ complex could not be experimentally distinguished from $Cu^I_4-S_6$ complex (*48*); thus, recruitment or coordination by His27, if present, may be difficult to ascertain from these spectra of C31S BxmR.

Ag^I Forms a Mononuclear Trigonal Planar Structure That Is Distinct from the Cd^{II} Complex. In contrast to Cu^I, titration of apo-BxmR with Ag^I gives rise to significant absorption in the UV region that appears to be saturable with just 1 mol equiv of the ion (spectra not shown). Perturbed angular correlation (PAC) spectroscopy was used to investigate the structure of the Ag^I complex in more detail and determine how this structure differs from that of Cd^{II} complex. ^{111}Ag decays to ^{111m}Cd and in the PAC measurement the nuclear quadrupole interaction (NQI)[1] between the cadmium nucleus and the surrounding charge distribution is recorded (*49*). It is assumed that the electronic relaxation after the nuclear decay is very fast on the PAC (nsec) time scale, but the structural relaxation from Ag^I coordination geometry to Cd^{II} coordination geometry may appear fast, intermediate, or slow on this time scale. This can be tested by comparing ^{111}Ag and ^{111m}Cd PAC spectra on the same protein. If they differ from one another, it is an indication that the structural relaxation is slow. Inspection of Figure 6A−C reveals that there appears to be no trace of the ^{111m}Cd-BxmR PAC spectrum (Figure 6C) in the ^{111}Ag-BxmR PAC spectrum (Figure 6A,B); this suggests that the lifetime of the Ag^I-coordination geometry is sufficiently long as to allow for observation of the Ag^I-coordination complex without complications of decay to the Cd^{II} complex.

The Fourier transform of the Ag^I-BxmR perturbation function (Figure 6D,E) reveals two main features, one at 0.23 rad/ns and one at ≈0.4 rad/ns. Since the ≈0.4 rad/ns peak has a higher amplitude than the peak at about 0.23 rad/ns, this strongly indicates that more than one NQI and thus more than one coordination environment are present in the Ag^I complex. The NQI with ω_0 about 0.220 rad/ns (Table 2) can be extracted with reasonable certainty, as all three peaks (at about 0.220, 0.410, and 0.630 rad/ns, respectively) are present beyond the noise in the Fourier transform, and they obey the rule $\omega_1 + \omega_2 = \omega_3$; this is valid as the intermediate nuclear level has a spin of $^5/_2$ (*50*). The second NQI shown in Table 2 is less reliable and difficult to extract, and two possibilities (fit 1 and fit 2, Figure 6D,E) give almost the same reduced χ^2 when fit. These two NQIs both reproduce the low intensity peak at about 0.820 rad/ns observed at approximately twice the frequency of the most intense peak in the Fourier transform. This indicates that the corresponding NQI either has η close to 1 (Table 2 and Figure 6D, fit 1) or η close to 0 (Table 2 and Figure 6E, fit 2). It is a classic problem in PAC spectroscopy that these two cases are difficult to distinguish (*51*).[3] The fact that two significantly different NQIs are observed reveals two different coordination environments are present in solution for Ag^I-BxmR, at least at a Ag^I:protein ratio of about 1:10. Although the NQIs with ω_0 at 0.220 rad/ns may represent a variety of coordination geometries, the NQI with ω_0 about 0.420 rad/ns and low η is diagnostic for a trigonal planar coordination geometry composed of three coordinating cysteines.[4]

Although visual inspection of the Cd-BxmR spectrum (Figure 6C,F) seems to be indicative of only one NQI with a relatively high value of η, it is not possible to make a satisfactory fit of the data with just one NQI. Indeed, addition of a second NQI reduced χ^2 is reduced significantly (*51*) (by about 0.4). Thus the fit was carried out with two NQIs which, not surprisingly, turn out to be very similar (Table 2). This indicates that the two symmetry-related α3N sites in Cd^{II}-BxmR adopt similar coordination geometries at a Cd^{II}:protein ratio of ≈1:5. The relatively low values of ω_0 might indicate the coordination geometries deviate markedly from perfect tetrahedral symmetry, assuming that only cysteine ligands are present (see Figure S2).

Regulation of Operator-Promoter (O/P) DNA Binding of BxmR by Different Metal Ions. The above metal binding experiments with wild-type and mutant BxmRs establish the

[3] Other fits may give equally good reduced χ^2 values but will not reproduce the low intensity peak at about 0.82 rad/ns in Figure 6D,E. A number of parameters were fixed in the fit in order to force the fit to include the considerations described in the text. Floating all parameters did not significantly change the reduced χ^2.

[4] We note that, as a control, we also carried out a ^{111}Ag PAC experiment on precipitated AgCl. This spectrum is clearly different (data not shown) from that observed in the Ag-BxmR; thus, it is reasonable to assume that the PAC signal deriving the Ag^I-BxmR complex does indeed originate from Ag^I bound to BxmR.

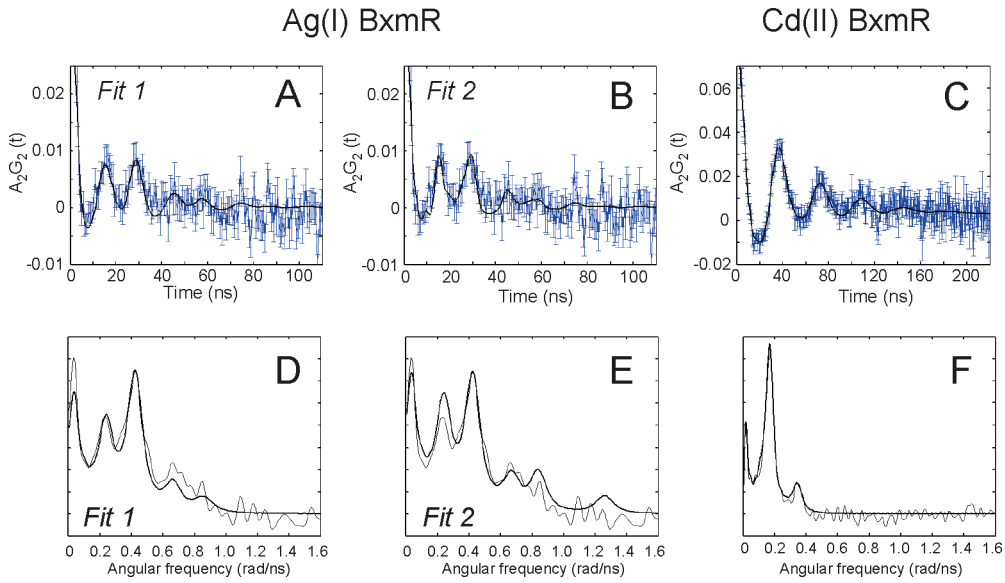

FIGURE 6: ^{111}Ag and ^{111m}Cd perturbed angular correlation (PAC) spectroscopy of Ag^{I}-substituted and Cd^{II}-substituted wild-type (WT) BxmR, respectively. Top (panels A and B, ^{111}Ag PAC; panel C, ^{111m}Cd PAC): the experimentally determined perturbation function (with error bars, in blue) and fit (boldfaced black line). Bottom (panels D−F): Fourier transformations of the experimental perturbation function in panels A−C, respectively (thin line) and fit (boldfaced line). The data from ^{111}Ag PAC experiments in panels A and B are identical and merely show the results of two independent fits (1 and 2; see Table 2); these are multiplied by −1 to allow for easy comparison with ^{111m}Cd PAC data (panel C). Parameters that derive from the fitted curves are compiled in Table 2.

Table 2: PAC Fitted Parameters for ^{111}Ag and ^{111m}Cd Bound to *O. brevis* BxmR[a]

protein	ω_0 (rad/ns)	η	$\Delta\omega_0/\omega_0 \times 100$	$A \times 100$	χ_r^2
Ag-BxmR: Fit 1	0.217 (3)	0.33 (4)	2f	2.1 (3)	1.11
	0.245f	1f	2f	1.6 (4)	
Ag-BxmR: Fit 2	0.221 (3)	0.32 (3)	2f	3.0 (2)	1.19
	0.420f	0.05f	2f	1.8 (2)	
Cd-BxmR	0.97 (4)	0.78 (19)	19 (3)	5.0 (6)	1.14
	0.101 (1)	0.89 (3)	6 (1)	2.9 (6)	

[a] The numbers in parentheses represent the standard deviations of the fitted parameters. "f" indicates that the parameter was fixed in the fit.

stoichiometry and affinity by which individual metal ions bind to the α3N and α5 sites on BxmR, as well as insights into their coordination environments. Previous studies establish that BxmR binds to a typical ArsR-family operator containing a 12-2-12 inverted repeat sequence situated just upstream of the *bxa1* gene encoding a CPx-ATPase (*36*). Figure 7 shows representative anisotropy-based *bxa1* O/P isotherms for wild-type (Figure 7A), α3NΔ BxmR (Figure 7B), and α5Δ BxmR (Figure 7C) carried out with apo-BxmR or with BxmRs preincubated with 1:1 (Zn^{II}, Cd^{II}, or Ag^{I}) or 2:1 (Cu^{I}) (per BxmR monomer) of the indicated metal ion (25 °C, pH 7.0, 0.2 M NaCl). The data were fit to a model assuming that two BxmR dimers bind to the operator with equal affinities (*36*), with the fitted parameters compiled in Table 3.

The data taken collectively reveal that *bxa1* O/P DNA binding activity of BxmR is allosterically negatively regulated by all four metals tested. Monovalent Cu^{I} and Ag^{I} as well as divalent Cd^{II} are equally effective in inhibiting DNA binding, with an allosteric coupling free energy, ΔG_c, of +1.7 (±0.1) kcal mol^{-1} under these conditions (Table 3). All three of these metals function through the thiophilic α3N metal binding site, since α3NΔ BxmR shows no regulation by Cd^{II} or Cu^{I} (Figure 7B). In striking contrast to Cu^{I} and Cd^{II}, Zn^{II} is unique in that this metal is a potent effector of *bxa1* O/P binding by α3NΔ BxmR, with a lower limit for ΔG_c of +3.4 (±0.1) kcal mol^{-1}; this result shows that Zn^{II} is capable of functioning through the α5 metal binding sites. Binding to the α5 sites is not obligatory, however, since Zn^{II} also negatively regulates DNA binding in α5Δ BxmR, i.e., through the α3N binding sites. Thus, BxmR retains a functional redundancy in its response to Zn^{II}, unlike all other metals that induce *bxa1* expression in *O. brevis* (*32*).

DISCUSSION

O. brevis BxmR is the fifth primary zinc-sensing member of the ArsR/SmtB family of metalloregulatory repressors (*33*) to be purified and characterized, four of which derive from different cyanobacterial species. The others are *Synechococcus* SmtB (*17*), *Synechocystis* ZiaR (*52*), *Anabaena* PCC7120 AztR (*8*), and *S. aureus* CzrA (*20, 53*). BxmR is most closely related on the basis of global amino acid sequence similarity to ZiaR, followed by AztR and SmtB (see Figures 1 and 8A), and these four proteins are part of a small cluster of sequences within the group 2 clade of ArsR-family repressors (*7*) (our data not shown; see Figure 8A). These sensors represent four of the ≈15 ArsR/SmtB sensors for which significant biochemical and cell biological data are now available, which collectively respond to an impressive range of metal ions including Zn^{II}, Zn^{II}/Co^{II}, Ni^{II}/Co^{II}, Cd^{II}/Pb^{II}, As^{III}/Sb^{III}, Bi^{III}, and Cu^{I}/Ag^{I} (*6, 14*) (see Figure 8B). In this report, we establish that BxmR is unique in this family of proteins in that despite the fact that Zn^{II} is the most potent inducer of *bxa1* expression (*33*), BxmR mediates a clear response to Cu^{I}/Ag^{I} both intracellularly and *in vitro* (*36*) in striking contrast to ZiaR (*52*).

Extensive biochemical, crystallographic, and NMR structural studies of CzrA, a Zn^{II}/Co^{II} sensor from *S. aureus*, the Cd^{II}/Pb^{II} sensor CadC from *S. aureus* pI258 and *L. monocytogenes*, *Synechococcus* SmtB and NmtR, the Ni^{II}/Co^{II} sensor from *M. tuberculosis*, establish the evolution of two distinct metal sensing sites (α3N and α5) on this ho-

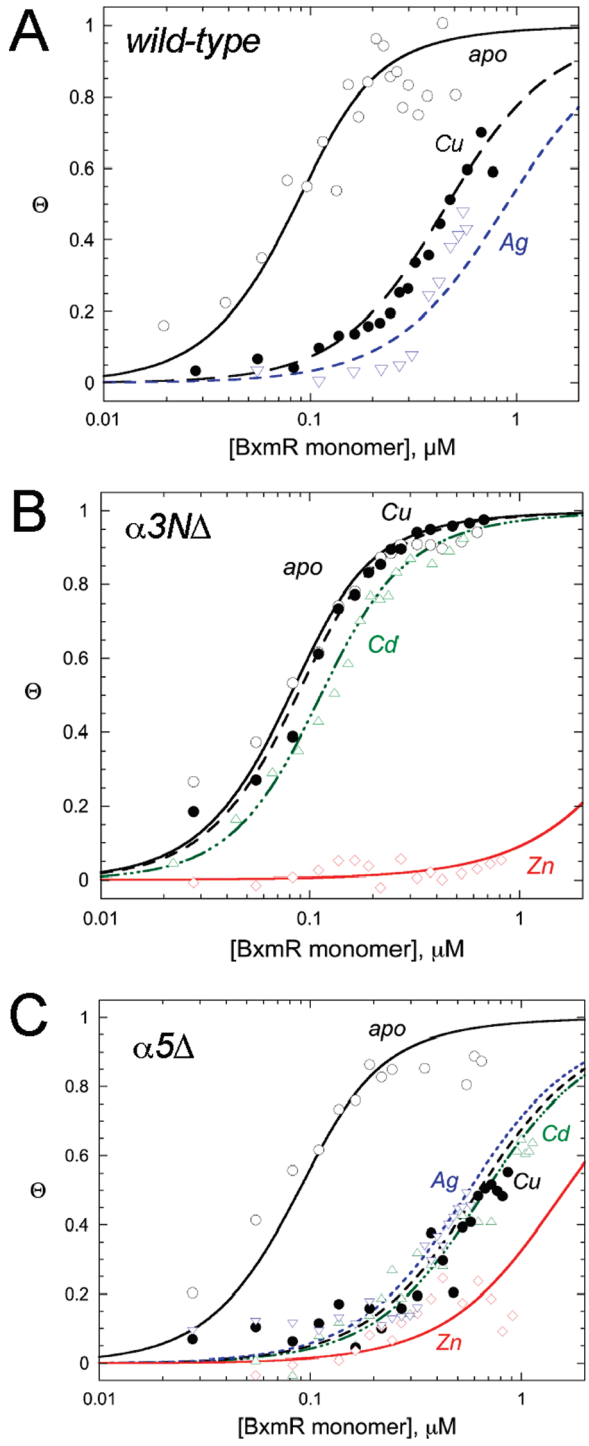

FIGURE 7: Representative normalized fluorescence anisotropy-based *bxa1* operator/promoter DNA binding isotherms for various WT (A), α3NΔ (B), and α5Δ (C) BxmRs in the absence (apo) and presence of the indicated metal ions. The continuous line through each binding isotherm represents a nonlinear least-squares fit to a two-dimer DNA binding model (see Experimental Procedures), with the fitted parameters compiled in Table 3.

Table 3: *bxa1* O/P Binding Parameters for Apo and Various Metal-Loaded States of Wild-Type, α3NΔ, and α5Δ BxmRs[a]

BxmR protein	metal	r_D	$r_{(P2)2•D}$	K_1 (M^{-1})	ΔG_c (kcal/mol)[b]
wild type	apo	0.108	0.135	1.0 (±0.2) × 10^8	
	$Cu^I_{1.8}$	0.106	0.135[c]	7.1 (±0.1) × 10^6	1.6
	Ag^I	0.108	0.135[c]	3.7 (±0.4) × 10^6	1.9
α3NΔ	apo	0.108	0.138	1.2 (±0.1) × 10^8	
	Cu^I	0.109	0.138	1.0 (±0.2) × 10^8	0.1
	Cd^{II}	0.113	0.135	7.2 (±0.1) × 10^7	0.3
	Zn^{II}	0.109	0.138[c]	≤5.0 (±0.3) × 10^5	≥**3.2**[d]
α5Δ	apo	0.109	0.137	1.0 (±0.2) × 10^8	
	Cu^I	0.106	0.137[c]	5.0 (±0.1) × 10^6	1.8
	Ag^I	0.105	0.137[c]	5.6 (±0.1) × 10^6	1.7
	Cd^{II}	0.111	0.137[c]	5.0 (±0.1) × 10^6	1.8
	Zn^{II}	0.110	0.137[c]	1.8 (±0.4) × 10^6	2.4

[a] Parameters determined from nonlinear least-squares fits of the data shown in Figure 7 using the model described under Experimental Procedures. [b] Estimated uncertainty in ΔG_c is ±0.1 kcal/mol. [c] This value of $r_{(P2)2•D}$ was fixed to the value obtained for the appropriate apoprotein in each case during the parameter optimization. The value of r_D was fixed to the experimentally measured value during parameter optimization. [d] Reflects a lower limit given the upper limit on K_1 (see Figure 7B for binding curve).

modimeric winged helical scaffold (Figure 8B) (*1, 3, 20, 21, 26, 30*). The α3N site is anchored by a pair of Cys likely positioned at the N-terminus of the α3 helix (Cys75 and Cys77 in BxmR) but shows considerable variability in the number and type of donor atoms that are known or predicted to make coordination bonds to the metal. Previous studies of *S. aureus* CadC established that a Gly substitution of the Cys corresponding to Cys77 in BxmR abrogates allosteric coupling of Cd^{II}/Pb^{II}/Zn^{II} binding to DNA binding by CadC and rendered CadC unable to sense metals *in vivo* (*45*); the analogous Ser substitution in AztR abolishes Zn^{II} sensing *in vivo* and Pb^{II} binding *in vitro* (*8*). Interestingly, the same Gly substitution occurs naturally in SmtB (see Figure 1); this substitution makes the prediction that the α3N site in SmtB would be capable of binding metals but would not be regulatory, and this is exactly in accord with experiment (*31*). Interestingly, *S. aureus* CadC contains both intact α3N and α5 metal sites, and the crystal structure of "apo-CadC" revealed that both α5 sites were filled with Zn^{II} (*1*), a finding consistent with its very high equilibrium affinity (L. Busenlehner and D. Giedroc, unpublished results). However, this site is *not* metalloregulatory for *cad* O/P binding, since an α3N inactivating mutation analogous to the one characterized here in α5Δ BxmR (C60G in CadC; C77S in BxmR) abolishes regulation of DNA binding by all metal ions (*30*). This property is in strong contrast to BxmR which retains potent Zn^{II} regulation through its α5 metal sites to a degree that is comparable to that of *bona fide* α5 zinc sensor *S. aureus* CzrA (*23, 41*).

It is striking that the four cyanobacterial zinc sensors have evolved distinct metal binding properties in a way that seems to track largely with differences in the N-terminal region. CadC contains an additional N-terminal α-helix (α0)[1] not found in α5 sensors SmtB (*3*), CzrA (*54*), or NmtR (A. Arunkumar, H. Reyes, and D. Giedroc, unpublished observations), with the most N-terminal residue visible in electron density maps Tyr12 (*1*). Tyr12 is just C-terminal to Cys7 and Cys11, the former of which donates a thiolate ligand to the Cd^{II}/Pb^{II} ion (*30*) and may well be required to drive a conformational change in the dimer that lowers the DNA-binding affinity of the repressor (*55*). ZiaR and AztR contain longer N-terminal domains (see Figure 1). Each contains a single Cys that aligns with the key allosteric residue Cys7 of CadC, as well as one conserved His (His27 in AztR). The α3N chelates of ZiaR and AztR are structurally indistinguishable and are consistent with an S_3(N/O) tetrahedral coordination environment as determined by the Co^{II} coordination complex, easily distinguished from the highly

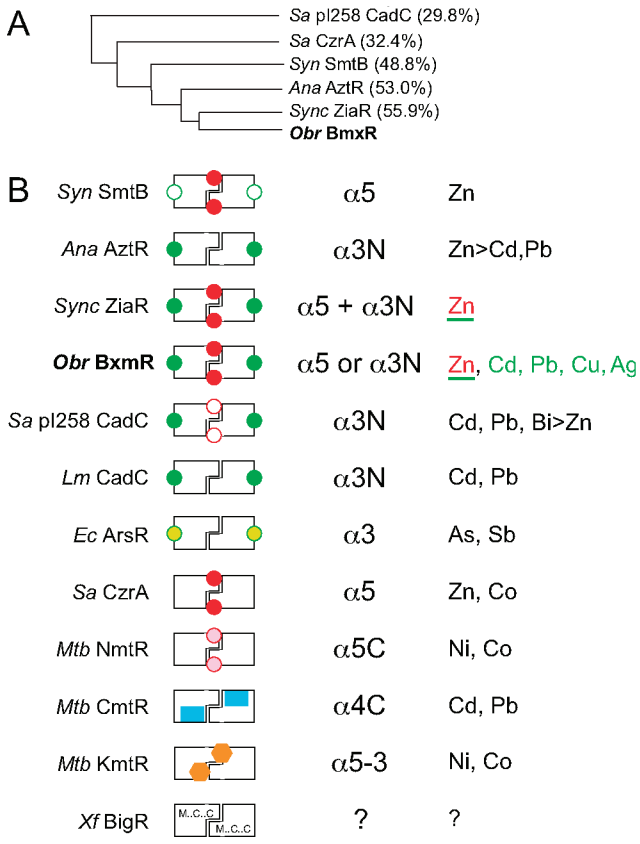

FIGURE 8: Schematic comparison of ArsR/SmtB family metal sensors with well-characterized metal binding properties. (A) Dendogram that illustrates the degree to which the four cyanobacterial ArsR/SmtB zinc sensors are related to one another and to previously characterized α5 (*Sa* CzrA) and α3N (*Sa* pI258 CadC) sensors on the basis of a global sequence similarity (% identity to *Obr* BxmR also indicated). (B) Schematic rendering of ArsR/SmtB sensors that highlights known regulatory metal sites (filled symbols) with their associated trivial designations (third column) and metal ions that are sensed *in vivo* (fourth column) by these sites. Other known metal sites that play no regulatory role are represented by open symbols (in *Syn* SmtB and *Sa* pI258 CadC). Sensors are *Synechococcus* (*Syn*) SmtB (*31, 57*), *Anabaena* (*Ana*) AztR (*8*), *Synechocystis* (*Sync*) ZiaR (*6, 52*), *O. brevis* (*Obr*) BxmR (this work), *S. aureus* (*Sa*) pI258 CadC (*30, 46*), *Listeria monocytogenes* (*Lm*) CadC (*30*), *E. coli* R773 (*Ec*) ArsR (*59*), *S. aureus* (*Sa*) CzrA (*3*), *M. tuberculosis* (*Mtb*) NmtR (*20, 60*), *M. tuberculosis* (*Mtb*) CmtR (*22, 24, 25*), *M. tuberculosis* (*Mtb*) KmtR (*7*), and *Xylella fastidiosa* (*Xf*) BigR (*27, 29*). For *Obr* BxmR, the metals sensed by the α3N site are shaded green; Zn^{II} is sensed by both α5 and α3N sites (this work); for ZiaR, both sites are apparently required to sense Zn^{II} *in vivo* (*52*). Although the inducer identity of *Xf* BigR is not yet known (?), BigR contains conserved Met, Cys, and Cys residues in the projected α1, α2, and α5 helices (*27*). See text for additional details.

distorted S_4 site of CadC (*8*). BxmR contains the longest N-terminal extension of any cyanobacterial ArsR-family Zn^{II} sensor to date (see Figure 1). BxmR conserves the key Cys corresponding to Cys7 in CadC (Cys23) but also contains three additional candidate metal ligands: a His analogous to His18 in SmtB (this His is proposed to donate a ligand to the α3N-bound Zn^{II} in SmtB *21, 43*), a unique Cys (Cys31) not found in the other sensors, and His15, analogous to Cys12 in ZiaR (see Figure 1). The Co^{II} spectrum of Co^{II}-substituted α5Δ BxmR is very similar to Co^{II}-AztR and is thus consistent with S_3(N/O) α3N site (*8*); however, the Cd^{II} complex contains 3−4 thiolate ligands, with the unique Cys31 apparently making a coordination bond (Supporting Information Figures S2 and S3).

The distinct N-terminal region of BxmR stably accommodates an α3N Cu^I complex in a solvent-shielded (*38*) binuclear Cu_2S_4 cluster that we propose involves Cys23, Cys31, Cys75′, and Cys77′ as wild-type metal ligands. This proposed binuclear copper cluster structure appears analogous to that proposed for Cu^I-specific sensor *Enterococcus* CopY (*56*). Each of the Cu^I ions in BxmR is trigonally coordinated with three Cu−S^- distances at 2.26 Å and a single Cu−Cu distance of 2.70 Å (see Figure 5); essentially identical spectra are obtained with the WT and α5Δ BxmR consistent with the conclusion that the C-terminal α5 site plays no role in Cu^I binding or Cu^I-dependent negative allosteric regulation of DNA binding (Figure 7). We note however, that Cu^I binds to BxmR with an average stepwise binding affinity of $\approx 1 \times 10^7\ M^{-1}$ (Figure 4A), which is quite weak relative to other known mononuclear bacterial Cu^I sensors *E. coli* CueR (*19*) and *M. tuberculosis* CsoR (*37*) as well as the multinuclear Cu^I complex in *Drosophila* MTF-1 (*38*). This finding is consistent with the idea that the α3N site in BxmR is not selective for Cu^I and may have resulted from the use of copper salts as algaecides for *O. brevis* used in these studies (*33*). These physical data show conclusively that residues derived from the N-terminal domain of BxmR allow direct binding of monovalent ions Cu^I/Ag^I in a way that induces negative regulation of DNA binding to a degree that is identical to divalent ions Zn^{II}/Cd^{II}. These findings provide additional evidence that the α3N site is structurally plastic and particularly well-suited to adopt a wide range of coordination chemistries (geometries and stoichiometries) to accommodate a wider range of metal ions and thereby mediate their homeostasis under conditions of metal ion excess (*30*).

A side-by-side comparison of the physical properties of the four closely related zinc-sensing ArsR/SmtB repressors (*Syn* SmtB, *Ana* AztR, *Obr* BxmR, and *Sync* ZiaR) reveals the remarkable finding that each likely utilizes a distinct structural mechanism to mediate resistance to toxic concentrations of Zn^{II} in the cell (see Figure 8). A similar conclusion was reached on the basis of a comparison of three As^{III}-sensing ArsRs, each of which harbors distinct S_3 coordination sites proposed to result from convergent evolution in response to recent environmental pressures (*5*). We note that *Anabaena* contains one other ArsR/SmtB regulator, most closely related to *Syn* SmtB termed AzuR (alr0831) not listed in Figure 8B; AzuR has been proposed to be a Zn^{II} uptake repressor (*8*), but this has not yet been tested experimentally.[5] In any case, *Syn* SmtB (and likely *Ana* AzuR) utilizes a single pair of subunit bridging α5 metal sites (*31, 57*) much like *Sa* CzrA (*23*). In AztR, the α5 metal sites have been lost, and as a result, Zn^{II} regulation falls to the CadC-like S_3(N/O) α3N sites (*8*). AztR also senses Cd^{II}/Pb^{II} through these metal sites, but the metal effluxer whose expression is regulated by AztR, AztA, is largely functionally selective for Zn^{II} (*58*). In

[5] Like SmtB, AzuR contains a naturally occurring nonliganding Ser in the α3 CV**S** sequence (analogous to C74S AztR (*8*) and C77S BxmR characterized here); this is predicted to inactivate Zn^{II} sensing at this site. Recent studies show that AzuR binds a single monomer mol equiv of Zn^{II}/Co^{II} with high affinity to form a tetrahedral $(N/O)_4$ α5 site complex and is therefore structurally indistinguishable from *Sa* CzrA (Z. Ma, R. Scott, and D. Giedroc, unpublished observations) (*3*).

contrast, *Obr* BxmR can exploit *either* α5 or α3N metal sites to effect zinc regulation, with the Zn^{II}-bound α5 sites far more selective and far more effective in allosterically inhibiting operator/promoter DNA binding. Finally, *in vivo* experiments suggest that *Sync* ZiaR requires *both* α5 and α3N metal sites to effect metalloregulation by Zn^{II} since inactivation of one or the other abolished Zn^{II} sensing in the cell (*52*); the structural basis for this is not yet known but would appear to be in contrast to BxmR. This feature might enhance the metal selectivity of ZiaR for Zn^{II} relative to AztR and BxmR since Cu^{I} and Ag^{I} do not induce the *zia* operon in *Synechocystis* cultures (*52*). It will be interesting to determine the extent to which the metallothionein BmtA and the metal transporter Bxa1 bind and transport, respectively, Ag^{I}/Cu^{I} vs Zn^{II}/Cd^{II}.

One common feature of all ArsR/SmtB sensors that have investigated in detail to date is that filling of one of two symmetry-related metal sites is necessary and sufficient to mediate regulation of DNA binding (*41*). For example, inactivation of one of the two pairs of sensing sites in BxmR to create α5Δ and α3NΔ BxmRs results in retention of a single high-affinity metal binding site with the second symmetry-related site on the homodimer characterized by a lower affinity for the metal (Table 1); a similar characteristic was found for all α5 first coordination shell mutants of *Sa* CzrA (*23*). Nonetheless, all drive approximately wild-type levels of regulation, at least *in vitro*. Current efforts are directed toward understanding in molecular terms how metal binding to the α5 vs the α3N sites drives negative allosteric regulation of DNA binding in BxmR and other ArsR family sensors and what factors dictate the quantitatively more potent regulation that occurs upon metal binding by the C-terminal α5 sites (*54*).

ACKNOWLEDGMENT

We thank Dr. Larry Dangott in the Protein Chemistry Laboratory at Texas A&M University for performing amino acid analysis on BxmR samples.

SUPPORTING INFORMATION AVAILABLE

Supplementary methods, the curve-fitting results from the Cu^{I} EXAFS experiments (Table S1), Zn^{II} binding data for the α3NΔ and α5Δ BxmRs (Figure S1), spectral data for the Co^{II}- (Figure S2) and Cd^{II}- (Figure S3) substituted wild-type and mutant BxmRs, and the spectrum obtained after 1.1 mol equiv of Co^{II} is added to Cu^{I}_{2}-C31S BxmR (Figure S4). This material is available free of charge via the Internet at http://pubs.acs.org.

REFERENCES

1. Ye, J., Kandegedara, A., Martin, P., and Rosen, B. P. (2005) Crystal structure of the *Staphylococcus aureus* pI258 CadC Cd(II)/Pb(II)/Zn(II)-responsive repressor. *J. Bacteriol. 187*, 4214–4221.
2. Cook, W. J., Kar, S. R., Taylor, K. B., and Hall, L. M. (1998) Crystal structure of the cyanobacterial metallothionein repressor SmtB: a model for metalloregulatory proteins. *J. Mol. Biol. 275*, 337–346.
3. Eicken, C., Pennella, M. A., Chen, X., Koshlap, K. M., VanZile, M. L., Sacchettini, J. C., and Giedroc, D. P. (2003) A metal-ligand-mediated intersubunit allosteric switch in related SmtB/ArsR zinc sensor proteins. *J. Mol. Biol. 333*, 683–695.
4. Qin, J., Fu, H. L., Ye, J., Bencze, K. Z., Stemmler, T. L., Rawlings, D. E., and Rosen, B. P. (2007) Convergent evolution of a new arsenic binding site in the ArsR/SmtB family of metalloregulators. *J. Biol. Chem. 282*, 34346–34355.
5. Ordoñez, E., Thiyagarajan, S., Cook, J. D., Stemmler, T. L., Gil, J. A., Mateos, L. M., and Rosen, B. P. (2008) Evolution of metal(loid) binding sites in transcriptional regulators. *J. Biol. Chem. 283*, (in press).
6. Busenlehner, L. S., Pennella, M. A., and Giedroc, D. P. (2003) The SmtB/ArsR family of metalloregulatory transcriptional repressors: Structural insights into prokaryotic metal resistance. *FEMS Microbiol. Rev. 27*, 131–143.
7. Campbell, D. R., Chapman, K. E., Waldron, K. J., Tottey, S., Kendall, S., Cavallaro, G., Andreini, C., Hinds, J., Stoker, N. G., Robinson, N. J., and Cavet, J. S. (2007) Mycobacterial cells have dual nickel-cobalt sensors: sequence relationships and metal sites of metal-responsive repressors are not congruent. *J. Biol. Chem. 282*, 32298–32310.
8. Liu, T., Golden, J. W., and Giedroc, D. P. (2005) A zinc(II)/lead(II)/cadmium(II)-inducible operon from the cyanobacterium *Anabaena* is regulated by AztR, an α3N ArsR/SmtB metalloregulator. *Biochemistry 44*, 8673–8683.
9. Outten, C. E., and O'Halloran, T. V. (2001) Femtomolar sensitivity of metalloregulatory proteins controlling zinc homeostasis. *Science 292*, 2488–2492.
10. O'Halloran, T. V. (1993) Transition metals in control of gene expression. *Science 261*, 715–725.
11. Finney, L. A., and O'Halloran, T. V. (2003) Transition metal speciation in the cell: insights from the chemistry of metal ion receptors. *Science 300*, 931–936.
12. Silver, S., and Phung, L. T. (1996) Bacterial heavy metal resistance: new surprises. *Annu. Rev. Microbiol. 50*, 753–789.
13. Barkay, T., Miller, S. M., and Summers, A. O. (2003) Bacterial mercury resistance from atoms to ecosystems. *FEMS Microbiol. Rev. 27*, 355–384.
14. Giedroc, D. P., and Arunkumar, A. I. (2007) Metal sensor proteins: nature's metalloregulated allosteric switches. *Dalton Trans.* 3107–3120.
15. Hobman, J. L., Wilkie, J., and Brown, N. L. (2005) A design for life: prokaryotic metal-binding MerR family regulators. *Biometals 18*, 429–436.
16. San Francisco, M. J., Hope, C. L., Owolabi, J. B., Tisa, L. S., and Rosen, B. P. (1990) Identification of the metalloregulatory element of the plasmid-encoded arsenical resistance operon. *Nucleic Acids Res. 18*, 619–624.
17. Morby, A. P., Turner, J. S., Huckle, J. W., and Robinson, N. J. (1993) SmtB is a metal-dependent repressor of the cyanobacterial metallothionein gene *smtA*: identification of a Zn inhibited DNA-protein complex. *Nucleic Acids Res. 21*, 921–925.
18. Iwig, J. S., Leitch, S., Herbst, R. W., Maroney, M. J., and Chivers, P. T. (2008) Ni(II) and Co(II) sensing by *Escherichia coli* RcnR. *J. Am. Chem. Soc. 130*, 7592–7606.
19. Changela, A., Chen, K., Xue, Y., Holschen, J., Outten, C. E., O'Halloran, T. V., and Mondragon, A. (2003) Molecular basis of metal-ion selectivity and zeptomolar sensitivity by CueR. *Science 301*, 1383–1387.
20. Pennella, M. A., Shokes, J. E., Cosper, N. J., Scott, R. A., and Giedroc, D. P. (2003) Structural elements of metal selectivity in metal sensor proteins. *Proc. Natl. Acad. Sci. U.S.A. 100*, 3713–3718.
21. VanZile, M. L., Chen, X., and Giedroc, D. P. (2002) Structural characterization of distinct α3N and α5 metal sites in the cyanobacterial zinc sensor SmtB. *Biochemistry 41*, 9765–9775.
22. Cavet, J. S., Graham, A. I., Meng, W., and Robinson, N. J. (2003) A cadmium-lead-sensing ArsR-SmtB repressor with novel sensory sites. Complementary metal discrimination by NmtR and CmtR in a common cytosol. *J. Biol. Chem. 278*, 44560–44566.
23. Pennella, M. A., Arunkumar, A. I., and Giedroc, D. P. (2006) Individual metal ligands play distinct functional roles in the zinc sensor *Staphylococcus aureus* CzrA. *J. Mol. Biol. 356*, 1124–1136.
24. Wang, Y., Hemmingsen, L., and Giedroc, D. P. (2005) Structural and functional characterization of *Mycobacterium tuberculosis* CmtR, a PbII/CdII-sensing SmtB/ArsR metalloregulatory repressor. *Biochemistry 44*, 8976–8988.
25. Banci, L., Bertini, I., Cantini, F., Ciofi-Baffoni, S., Cavet, J. S., Dennison, C., Graham, A. I., Harvie, D. R., and Robinson, N. J. (2007) NMR structural analysis of cadmium sensing by winged helix repressor CmtR. *J. Biol. Chem. 282*, 30181–30188.
26. Pennella, M. A., and Giedroc, D. P. (2005) Structural determinants of metal selectivity in prokaryotic metal-responsive transcriptional regulators. *Biometals 18*, 413–428.

27. Barbosa, R. L., and Benedetti, C. E. (2007) BigR, a transcriptional repressor from plant-associated bacteria, regulates an operon implicated in Biofilm growth. *J. Bacteriol. 189*, 6185–6194.
28. Rother, D., Orawski, G., Bardischewsky, F., and Friedrich, C. G. (2005) SoxRS-mediated regulation of chemotrophic sulfur oxidation in *Paracoccus pantotrophus*. *Microbiology 151*, 1707–1716.
29. Barbosa, R. L., Rinaldi, F. C., Guimaraes, B. G., and Benedetti, C. E. (2007) Crystallization and preliminary X-ray analysis of BigR, a transcription repressor from *Xylella fastidiosa* involved in Biofilm formation. *Acta Crystallogr. 63*, 596–598.
30. Busenlehner, L. S., Weng, T. C., Penner-Hahn, J. E., and Giedroc, D. P. (2002) Elucidation of primary (α3N) and vestigial (α5) heavy metal-binding sites in *Staphylococcus aureus* pI258 CadC: evolutionary implications for metal ion selectivity of ArsR/SmtB metal sensor proteins. *J. Mol. Biol. 319*, 685–701.
31. VanZile, M. L., Chen, X., and Giedroc, D. P. (2002) Allosteric negative regulation of *smt* O/P binding of the zinc sensor, SmtB, by metal ions: a coupled equilibrium analysis. *Biochemistry 41*, 9776–9786.
32. Liu, T., Nakashima, S., Hirose, K., Uemura, Y., Shibasaka, M., Katsuhara, M., and Kasamo, K. (2003) A metallothionein and CPx-ATPase handle heavy-metal tolerance in the filamentous cyanobacterium *Oscillatoria brevis*. *FEBS Lett. 542*, 159–163.
33. Tong, L., Nakashima, S., Shibasaka, M., Katsuhara, M., and Kasamo, K. (2002) A novel histidine-rich CPx-ATPase from the filamentous cyanobacterium *Oscillatoria brevis* related to multiple-heavy-metal cotolerance. *J. Bacteriol. 184*, 5027–5035.
34. Schrader, K. K., Nanayakkara, N. P., Tucker, C. S., Rimando, A. M., Ganzera, M., and Schaneberg, B. T. (2003) Novel derivatives of 9,10-anthraquinone are selective algicides against the musty-odor cyanobacterium *Oscillatoria perornata*. *Appl. Environ. Microbiol. 69*, 5319–5327.
35. Hirose, K., Ezaki, B., Liu, T., and Nakashima, S. (2006) Diamide stress induces a metallothionein BmtA through a repressor BxmR and is modulated by Zn-inducible BmtA in the cyanobacterium *Oscillatoria brevis*. *Toxicol. Lett. 163*, 250–256.
36. Liu, T., Nakashima, S., Hirose, K., Shibasaka, M., Katsuhara, M., Ezaki, B., Giedroc, D. P., and Kasamo, K. (2004) A novel cyanobacterial SmtB/ArsR family repressor regulates the expression of a CPx-ATPase and a metallothionein in response to both Cu(I)/Ag(I) and Zn(II)/Cd(II). *J. Biol. Chem. 279*, 17810–17818.
37. Liu, T., Ramesh, A., Ma, Z., Ward, S. K., Zhang, L., George, G. N., Talaat, A. M., Sacchettini, J. C., and Giedroc, D. P. (2007) CsoR is a novel *Mycobacterium tuberculosis* copper-sensing transcriptional regulator. *Nat. Chem. Biol. 3*, 60–68.
38. Chen, X., Hua, H., Balamurugan, K., Kong, X., Zhang, L., George, G. N., Georgiev, O., Schaffner, W., and Giedroc, D. P. (2008) Copper sensing function of *Drosophila* metal-responsive transcription factor-1 is mediated by a tetranuclear Cu(I) cluster. *Nucleic Acids Res. 36*, 3128–3138.
39. Walkup, G. K., and Imperiali, B. (1997) Fluorescent chemosensors fr divalent zinc based on zinc finger domains. Enhanced oxidative stability, metal binding affinity, and structural and functional characterization. *J. Am. Chem. Soc. 199*, 3443–3450.
40. Jefferson, J. R., Hunt, J. B., and Ginsburg, A. (1990) Characterization of indo-1 and quin-2 as spectroscopic probes for Zn2(+)-protein interactions. *Anal. Biochem. 187*, 328–336.
41. Lee, S., Arunkumar, A. I., Chen, X., and Giedroc, D. P. (2006) Structural insights into homo- and heterotropic allosteric coupling in the zinc sensor *S. aureus* CzrA from covalently fused dimers. *J. Am. Chem. Soc. 128*, 1937–1947.
42. Kuzmic, P. (1996) Program DYNAFIT for the analysis of enzyme kinetic data: application to HIV proteinase. *Anal. Biochem. 237*, 260–273.
43. VanZile, M. L., Cosper, N. J., Scott, R. A., and Giedroc, D. P. (2000) The zinc metalloregulatory protein *Synechococcus* PCC7942 SmtB binds a single zinc ion per monomer with high affinity in a tetrahedral coordination geometry. *Biochemistry 39*, 11818–11829.
44. Busenlehner, L. S., Cosper, N. J., Scott, R. A., Rosen, B. P., Wong, M. D., and Giedroc, D. P. (2001) Spectroscopic properties of the metalloregulatory Cd(II) and Pb(II) sites of *S. aureus* pI258 CadC. *Biochemistry 40*, 4426–4436.
45. Sun, Y., Wong, M. D., and Rosen, B. P. (2001) Role of cysteinyl residues in sensing Pb(II), Cd(II), and Zn(II) by the plasmid pI258 CadC repressor. *J. Biol. Chem. 276*, 14955–14960.
46. Busenlehner, L. S., Apuy, J. L., and Giedroc, D. P. (2002) Characterization of a metalloregulatory bismuth(III) site in *Staphylococcus aureus* pI258 CadC repressor. *J. Biol. Inorg. Chem. 7*, 551–559.
47. Cobine, P., Wickramasinghe, W. A., Harrison, M. D., Weber, T., Solioz, M., and Dameron, C. T. (1999) The *Enterococcus hirae* copper chaperone CopZ delivers copper(I) to the CopY repressor. *FEBS Lett. 445*, 27–30.
48. Brown, K. R., Keller, G. L., Pickering, I. J., Harris, H. H., George, G. N., and Winge, D. R. (2002) Structures of the cuprous-thiolate clusters of the Mac1 and Ace1 transcriptional activators. *Biochemistry 41*, 6469–6476.
49. Bauer, R., Danielsen, E., Hemmingsen, L., Bjerrum, M. J., Hansson, O., and Singh, K. (1997) Interplay between oxidation state and coordination geometry of metal ions in azurin. *J. Am. Chem. Soc. 119*, 157–162.
50. Hemmingsen, L., Sas, K. N., and Danielsen, E. (2004) Biological applications of perturbed angular correlations of gamma-ray spectroscopy. *Chem. Rev. 104*, 4027–4062.
51. Hemmingsen, L., and Hansen, B. (1995) Bayes theorem applied to the selection of model in PAC spectroscopy. *Z. Natureforsch. A 51a*, 442–446.
52. Thelwell, C., Robinson, N. J., and Turner-Cavet, J. S. (1998) An SmtB-like repressor from *Synechocystis* PCC 6803 regulates a zinc exporter. *Proc. Natl. Acad. Sci. U.S.A. 95*, 10728–10733.
53. Kuroda, M., Hayashi, H., and Ohta, T. (1999) Chromosome-determined zinc-responsible operon *czr* in *Staphylococcus aureus* strain 912. *Microbiol. Immunol. 43*, 115–125.
54. Arunkumar, A. I., Pennella, M. A., Kong, X., and Giedroc, D. P. (2007) Resonance assignments of the metal sensor protein CzrA in the apo-, Zn2- and DNA-bound (42 kD) states. *Biomol. NMR Assign. 1*, 99–101.
55. Busenlehner, L. S., and Giedroc, D. P. (2006) Kinetics of metal binding by the toxic metal-sensing transcriptional repressor *Staphylococcus aureus* pI258 CadC. *J. Inorg. Biochem.*
56. Cobine, P. A., George, G. N., Jones, C. E., Wickramasinghe, W. A., Solioz, M., and Dameron, C. T. (2002) Copper transfer from the Cu(I) chaperone, CopZ, to the repressor, Zn(II)CopY: metal coordination environments and protein interactions. *Biochemistry 41*, 5822–5829.
57. Turner, J. S., Glands, P. D., Samson, A. C., and Robinson, N. J. (1996) Zn^{2+}-sensing by the cyanobacterial metallothionein repressor SmtB: different motifs mediate metal-induced protein-DNA dissociation. *Nucleic Acids Res. 24*, 3714–3721.
58. Liu, T., Reyes-Caballero, H., Li, C., Scott, R. A., and Giedroc, D. P. (2007) Multiple metal binding domains enhance the Zn(II) selectivity of the divalent metal ion transporter AztA. *Biochemistry 46*, 11057–11068.
59. Shi, W., Dong, J., Scott, R. A., Ksenzenko, M. Y., and Rosen, B. P. (1996) The role of arsenic-thiol interactions in metalloregulation of the *ars* operon. *J. Biol. Chem. 271*, 9291–9297.
60. Cavet, J. S., Meng, W., Pennella, M. A., Appelhoff, R. J., Giedroc, D. P., and Robinson, N. J. (2002) A nickel-cobalt-sensing ArsR-SmtB family repressor. Contributions of cytosol and effector binding sites to metal selectivity. *J. Biol. Chem. 277*, 38441–38448.

BI801313Y